Origin of Glass Transition of Poly(2-vinylpyridine). A Temperature- and Pressure-Dependent Dielectric Spectroscopy Study

P. Papadopoulos, D. Peristeraki, and G. Floudas*

Department of Physics, University of Ioannina, and Biomedical Research Institute (FORTH-BRI), P.O. Box 1186, 451 10 Ioannina, Greece

G. Koutalas and N. Hadjichristidis

Department of Chemistry, University of Athens, 157 71 Athens, Greece

Received July 15, 2004; Revised Manuscript Received August 3, 2004

ABSTRACT: The dynamics of poly(2-vinylpyridine) (P2VP) have been studied as a function of temperature (in the range from 123 to 453 K), pressure (0.1−270 MPa), and molecular weight (1.1×10^3−3.0×10^4 g/mol), using dielectric spectroscopy (DS) within the frequency range from 10^{-2} to 10^6 Hz. Structural methods (wide-angle X-ray scattering) have been employed in parallel with thermodynamic methods (pressure−volume−temperature). Three relaxation processes were found: two above the glass temperature (T_g) associated with the segmental (α-) process and a slower process with an apparent activation volume comparable to the monomer volume and another well below T_g, with an Arrhenius T dependence (β-process). The results from the dynamic study combined with the thermodynamic results revealed that both decreasing thermal energy and insufficient volume lead to glass formation at lower temperatures, with the former having the stronger effect at temperatures near T_g (i.e., values of the ratio of apparent activation energies at constant volume and constant pressure in the range $Q_V/Q_P \sim 0.6$−0.85 for the different temperatures and pressures investigated).

I. Introduction

The temperature (T) and pressure (P) dependence of the dynamics of amorphous polymers can provide useful information concerning the origin of the dynamic arrest of the segmental dynamics at a temperature known as the "glass transition" temperature (T_g).[1] In recent years, the effect of pressure has been more extensively studied due to the availability of new experimental devices. Early work by Williams[2] and Saito[3] has shown that pressure is the appropriate thermodynamic variable when the separation of relaxation processes with similar relaxation times is required. Pressure has also been applied in (i) type-A polymers (i.e., polymers with a dipole moment component along the backbone) aiming at understanding the local segmental and normal mode dynamics,[4−7] (ii) athermal block copolymers and homogeneous polymer blends, by studying the effect of pressurization on the dynamic miscibility/heterogeneity,[8−11] (iii) on the issue of polymer crystallization[12] and the associated kinetics,[13] and (iv) on the dynamics of shape-persistent polymers (i.e., "hairy-rod" macromolecules,[14,15] side-chain liquid crystalline polymers,[16] and synthetic polypeptides[17]) aiming at understanding the origin of glass transition in systems exhibiting intrinsic orientational order. Moreover, P-dependent measurements can answer the question whether the dynamics are only controlled by the available or "free" volume, as suggested by the free volume theories, or by temperature through the thermal energy k_BT as suggested by different "landscape" models.[16−23] By changing temperature alone, both thermal energy (k_BT) and volume are changing, making impossible the separation of the two effects. The T- and P-dependent dielectric spectroscopy (DS) measurements combined with independent PVT experiments enable an investigation of the segmental dynamics under "isodensity" conditions. Under such conditions, the relative contributions from volume and thermal energy can be separately discussed, and the origin of the dynamic arrest at T_g can be clarified.

In the present study, a series of poly(2-vinylpyridine) (P2VP) samples with narrow molecular weight distributions are investigated with T- and P-dependent DS. Structural methods (wide-angle X-ray scattering, WAXS) have also been employed to characterize the packing efficiency together with thermodynamic methods (pressure−volume−temperature, PVT). The thermodynamic results coupled with the dynamic results provide an "activation energy map" that gives the relative contributions of volume and temperature on the segmental dynamics. We found that while the dynamics are affected both by volume and temperature, temperature is the main controlling parameter of the segmental dynamics in P2VP, especially when approaching T_g.

II. Experimental Section

Samples. Three poly(2-vinylpyridine) samples with number-averaged molecular weights of 1.1×10^3 (P2VP-A), 9.0×10^3 (P2VP-B), and 3.0×10^4 g/mol (P2VP-C) were synthesized by anionic polymerization of 2-vinylpyridine, using high-vacuum techniques, with *n*-BuLi as initiator. All apparatuses were washed with THF solution of *n*-BuLi (Aldrich) and 1,1-diphenylethylene (Aldrich) in a 1/5 molar ratio, followed by rinsing with THF, which was the solvent for all polymerizations. After purification, 2-vinylpyridine was distilled into the THF solution of the initiator and was polymerized for half an hour at 195 K. In Figure 1, the chemical structure of P2VP and a typical size exclusion chromatograph are shown. The molecular characteristics of the samples are given in Table 1.

Wide-Angle X-ray Scattering (WAXS). WAXS were made with a Siemens $\theta-\theta$ diffractometer. The Cu Kα radiation was used with a secondary graphite monochromator from a Siemens generator (Kristalloflex 710H) operating at 35 kV and 30 mA. The measurements were made within the q range from 1 to 28 nm^{-1} from room temperature up to 433 K. Figure 2

10.1021/ma048555s CCC: $27.50
Published on Web 09/22/2004

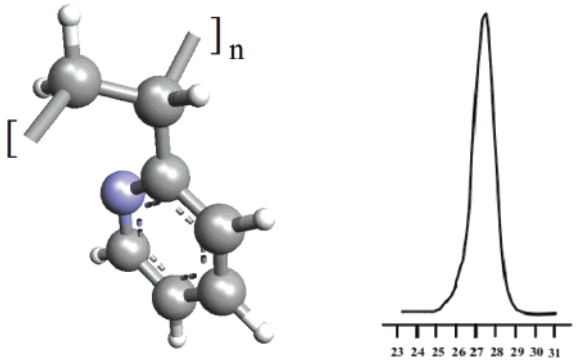

Figure 1. (left) Schematic model of the repeat unit of poly(2-vinylpyridine) (P2VP). (right) SEC chromatograph of P2VP-B.

Table 1. Molecular Characteristics and Glass Transition Temperatures of the Three Samples Investigated

sample	M_w (g/mol)	M_w/M_n	T_g^{DS} (K)
P2VP-A	1.1×10^3	1.10	332 ± 2.9
P2VP-B	9.0×10^3	1.09	340 ± 0.9
P2VP-C	3.0×10^4	1.04	366.8 ± 0.7

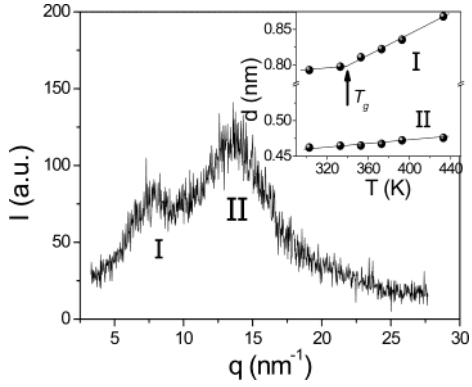

Figure 2. WAXS spectrum of P2VP-B at 303 K. The distances corresponding to the two broad peaks, marked I and II, are shown in the inset as a function of temperature. The high-q peak, known as the van der Waals (VDW) peak, arises from the VDW contacts of the atoms and has a weak temperature dependence. The low-q peak, known as low van der Waals peak (LVDW), corresponds to interchain distances and is related to the expansion coefficient, which rises significantly above T_g.

gives the diffraction pattern of P2VP-B at 303 K. The pattern is characterized by an intense peak (II) at $q \sim 14$ nm^{-1} (with a corresponding distance of 0.45 nm) and by a less intense peak (I) at $q \sim 8.5$ nm^{-1} (corresponding distance of 0.7 nm). Peak II is known as the van der Waals (VDW) peak and is considered to arise from the VDW contacts of atoms. Peak I is known as the low van der Waals (LVDW) peak and reflects interchain correlations.[24] This assignment is confirmed by their distinct T dependence[25] (shown in the inset), revealing that the LVDW peak is more sensitive to interchain correlations and thus to the T_g (the $\partial \ln d(T)/\partial T$ assumes values of 2×10^{-4} and 8.8×10^{-4} K^{-1} below and above T_g, respectively).

Pressure−Volume−Temperature Measurements (PVT). A fully automated GNOMIX high-pressure dilatometer was used for the PVT measurements (made by A. Best at the MPI-P, Mainz). At first, "isothermal" runs were performed by changing P in the range form 10 to 200 MPa and for temperatures in the range from 303 to 413 K. These measurements were followed by "isobaric" heating/cooling experiments for pressures in the range from 10 to 200 MPa. The results from the "isobaric" measurements are depicted in Figure 3. The change in the specific volume, $V(T)$, indicates the glass temperature that is increasing function of pressure. The

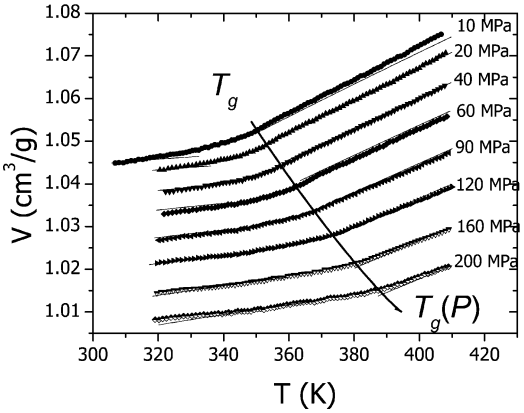

Figure 3. Specific volume obtained under "isobaric" conditions as a function of temperature and pressure. The change in the slope of the $V(T)$ curves indicates the pressure-dependent glass transition. The arrow shows the $T_g(P)$ dependence. Solid lines are the results of the fit of $V(T,P)$ to the Tait equation (eq 1).

regions below and above the transition regime have been fitted using the empirical Tait equation:

$$V(P,T) = V(0,T)(1 - 0.0894 \ln(1 - P/B(T))) \qquad (1)$$

where $V(0,T) = 1.024 + 4.2 \times 10^{-4}\, T - 2.0 \times 10^{-7}\, T^2$ and $B(T) = 278.9e^{-9.5\times10^{-4}T}$ (V in g cm^{-3}, T in °C, P in MPa).

Dielectric Spectroscopy. The T-dependent dielectric measurements were made using a Novocontrol BDS system composed of a frequency response analyzer, a broadband dielectric converter, and a cryostat operating in the T range of 193−423 K. The sample cell consisted of two 20 mm diameter electrodes between which a 50 μm thick sample was placed. The P-dependent measurements were made using a setup[26] consisting of a temperature-controlled high-pressure cell, a pump for hydrostatic pressure, and a closing press with pump. Pressure was applied using silicone oil as the transducing medium. The sample cell again consisted of two metal electrodes 20 mm in diameter with a 50 μm sample between them, which was sealed and placed inside a Teflon ring in order to prevent contact with the oil. The same BDS system as with the T-dependent measurements was used for the P-dependent measurements. Measurements were made under "isothermal" conditions (the following temperatures were used: 383, 393, 398, 403, 408, 413, 423, 433, 443, and 453 K) and for pressures in the range from 0.1 to 270 MPa. From these measurements the complex permittivity $\epsilon^* = \epsilon' - i\epsilon''$ was obtained as a function of frequency, temperature, and pressure $\epsilon^* = \epsilon^*(\omega,T,P)$. Figure 4 provides representative spectra under "isobaric" (0.1 MPa) and "isothermal" (403 K) conditions. The main process in the figure corresponds to the segmental (α-) process. At lower temperatures a weak β-process exists, whereas at high temperatures a slower process affects the dynamic response, and at even higher T/lower frequencies there is a strong conductivity contribution. The spectra were analyzed using the empirical equation of Havriliak and Negami:[27]

$$\frac{\epsilon^*(\omega,T,P) - \epsilon_\infty(T,P)}{\Delta\epsilon(T,P)} = \frac{1}{[1 + (i\omega\tau_{HN}(T,P))^a]^\gamma} \qquad (2)$$

where $\epsilon_\infty(T,P)$ is the dielectric permittivity at high frequencies, τ_{HN} is the characteristic relaxation time in this equation, $\Delta\epsilon = \epsilon_s - \epsilon_\infty$ is the dielectric strength of the process, and α, γ describe the symmetric and asymmetric broadening of the relaxation times distribution, respectively. In the fitting procedure the ϵ'' values were used and in some cases also the ϵ' values. The sample conductivity causes an increase of ϵ'' at low frequencies ($\epsilon'' \sim \sigma_0/(\epsilon_0\omega)$, where σ_0 is the dc conductivity and ϵ_0 the permittivity of free space) and has also been included in the fitting procedure. Because of the strong

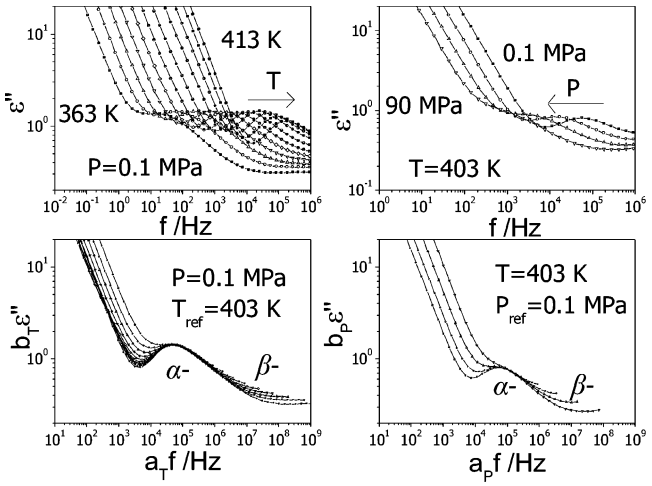

Figure 4. (top left) DS spectra obtained at 0.1 MPa and different temperatures: (■) $T = 363.15$ K, (○) $T = 368.15$ K, (△) $T = 373.15$ K, (▽) $T = 378.15$ K, (◇) $T = 383.15$ K, (△) $T = 388.15$ K, (▽) $T = 393.15$ K, (◐) $T = 398.15$ K, (▼) $T = 403.15$ K, (▲) $T = 408.15$ K, (●) $T = 413.15$ K. (bottom left) Superposition of the "isobaric" $\epsilon''(f)$ curves with respect to a reference curve at 403 K. (top right) DS spectra obtained at 403 K and variable pressures: (■) $P = 0.1$ MPa, (○) $P = 30$ MPa, (▲) $P = 60$ MPa, (▼) $P = 90$ MPa. (bottom right) Superposition of the "isothermal" loss curves with respect to a reference curve at 0.1 MPa.

conductivity contribution, to explore the $\tau(T,P)$ of the slower process, we have used the derivative method,[28] which provides an accurate estimate of $\tau(T,P)$ by calculating $\epsilon''_{der} = -\pi/2(\partial\epsilon'/\partial \ln \omega)$. This value is approximately equal to $\epsilon''(f)$ after removing the conductivity contribution. The frequency at maximum loss, f_{max}, is related to τ_{HN} by

$$f_{max} = \frac{1}{\tau_{HN}}\left(\frac{\sin\left(\frac{\pi\alpha}{2(\gamma+1)}\right)}{\sin\left(\frac{\pi\alpha\gamma}{2(\gamma+1)}\right)}\right)^{(1/\alpha)} \quad (3)$$

An alternative representation of the dielectric data is through the inverse of the dielectric permittivity $\epsilon^*(\omega)$, i.e., the electric modulus, related to the dielectric permittivity through

$$M^*(\omega) = \frac{1}{\epsilon^*(\omega)} = M' + iM'' \quad (4)$$

where M' and M'' are the real and imaginary parts of the electric modulus, respectively. The electric modulus representation (i.e., the decay of the electric field under conditions of constant dielectric displacement, D) rather than the complex permittivity (constant electric field, E) have been proposed not only for systems containing a substantial concentration of mobile carriers but also for any dielectrically active process. There are also cases where the use of $M^*(\omega)$ is an absolute necessity (i.e., comparison with rheology data). The relaxation times obtained from the electric modulus (τ_{M^*}) and the complex permittivity (τ_{ϵ^*}) representations scale as $\tau_{M^*}/\tau_{\epsilon^*} \sim \epsilon_\infty/\epsilon_s$ and can differ substantially in systems with high dielectric strengths.[29] On the other hand, in systems with weak processes the two times are nearly equal.

Finally, the dipole moments corresponding to the α-process were calculated. The dielectric strength, $\Delta\epsilon$, is directly related to the dipole moment through the equation $\Delta\epsilon = (4\pi FNg\mu^2/3k_BT)$, where μ is the dipole moment, N is the number of dipoles per unit volume, $F = (\epsilon_0(\epsilon_\infty + 2)^2/3(2\epsilon_0 + \epsilon_\infty))$ is the local field correction, and g is the Kirkwood−Fröhlich correlation factor due to neighboring dipoles. The effective dipole moment, defined as $\mu_{eff} = (g\mu^2)^{1/2}$, was found to be ∼1.2 D in all samples and T, P conditions.

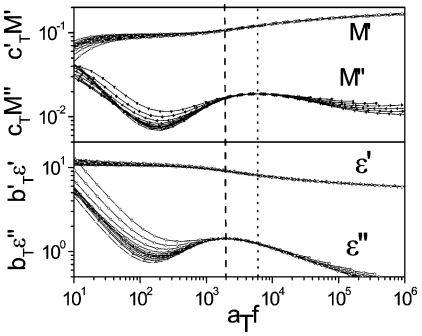

Figure 5. Superpositions of the real (M') and imaginary part (M'') of the electric modulus (top) and of the dielectric permittivity (ϵ') and loss curves (ϵ'')(bottom). The positions of the peaks (dashed and dotted lines give the positions of the ϵ'' and M'' maximum, respectively) differ by approximately half a decade due to the high dielectric intensity of the α-process. All relaxation times reported herein refer to the M'' maximum.

III. Results and Discussion

The dielectric loss spectra of P2VP-B shown in Figure 4 display a peak assigned to the segmental (α-) relaxation, under isobaric (at 0.1 MPa) and isothermal (at 403 K) conditions. Master curves were constructed from these data by multiplying the frequency axis of each curve by appropriate shift factors, a_T and a_P, at each T and P, so as to bring the dielectric loss maxima for the α-process in coincidence. The vertical axes have also been slightly shifted by corresponding factors b_T and b_P. The results of the attempted time−temperature ($t-T$s) and time−pressure superpositions ($t-P$s) are also shown in Figure 4 (bottom). The constructed "master curves" indicate that $t-T-P$s works reasonably well only around the α-process maximum. At higher and lower frequencies, the superposition fails because of the presence of a "fast" β-process and of a "slower" component with distinctly different T dependencies (see below).

The superimposed M' and M'' data are shown together with the ϵ' and ϵ'' data in Figure 5 (at $P = 0.1$ MPa) around the α-relaxation maximum using the same horizontal shift factor a_T. The shape of the peak in the ϵ'' and M'' data is different with Havriliak−Negami shape parameters of $\alpha = 0.80 \pm 0.10$, $\gamma = 0.50 \pm 0.05$ and $\alpha = 0.65 \pm 0.10$, $\gamma = 0.42 \pm 0.05$, respectively. Notice that $\tau_{M''}/\tau_{\epsilon''} \sim 0.3$ as suggested by the ratio $\epsilon'_\infty/\epsilon'_s$. This enables us to obtain the $\tau_{M''}$ times from the corresponding $\tau_{\epsilon''}$ times by applying the Havriliak−Negami equation to the dielectric susceptibility data and multiplying $\tau_{\epsilon''}$ by a constant factor. The relaxation times presented in the figures to follow are all $\tau_{M''}$ times.

The relaxation times at the M'' maximum for the low temperature (β-; open symbols), the segmental (α-; filled symbols), and the slower process (half-filled symbols) for all the three samples are shown in Figure 6 at 0.1 MPa. The β-process has an Arrhenius T dependence (with HN shape parameters $\alpha = 0.23 \pm 0.03$, $\gamma = 1.0$) that can be described by

$$\tau_{max} = \tau_0 \exp\left(\frac{E}{kT}\right) \quad (5)$$

where τ_0 is the relaxation time limit at infinite temperature and E is the activation energy (∼53 kJ/mol in all samples). The intensity of the β-process is low ($T\Delta\epsilon \sim$ 100 K), suggesting a local motion of the pyridine side group and/or a reduced number of relaxing units. On the other hand, the segmental process displays the

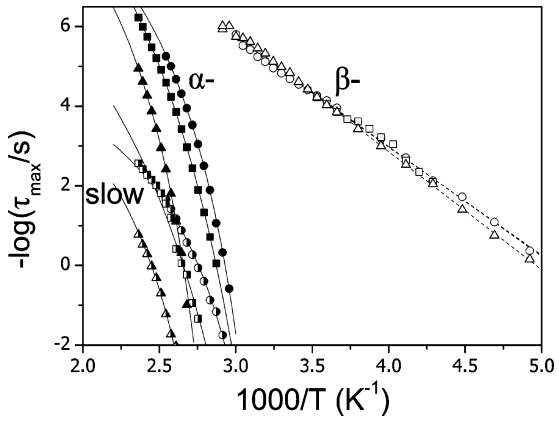

Figure 6. Relaxation times corresponding to the M'' maximum ($\tau_{M''}$) as a function of temperature (at 0.1 MPa) corresponding to the β-process (open symbols), the α-process (filled symbols), and the slower process (half-filled symbols) for the samples P2VP-A (circles), P2VP-B (squares), and P2VP-C (triangles). Solid and dashed lines are fits to the VFT (eq 6) and Arrhenius (eq 5) equations, respectively.

Table 2. *T*-Dependent VFT Parameters Corresponding to the α-Process

sample	$\log(\tau_0/\mathrm{s})$	D_T	T_0 (K)
P2VP-A	11.4 ± 0.3	6 ± 0.5	280 ± 2.5
P2VP-B	12.5 ± 0.3	9.2 ± 0.5	267 ± 0.7
P2VP-C	11.7 ± 0.1	6 ± 0.1	309 ± 0.5

usual strong $\tau(T)$ dependence according to the Vogel−Fulcher−Tammann (VFT) equation

$$\tau_{\max} = \tau_0 \exp\left(\frac{D_T T_0}{T - T_0}\right) \tag{6}$$

where D_T is a dimensionless parameter ($D_T = 9.2$ for P2VP-B) and T_0 is the "ideal" glass temperature. In DS, the glass transition temperature is operationally defined as the temperature where the segmental mode relaxation time is at 100 s. The slower process has also a VFT dependence (with HN shape parameters $\alpha = 0.75$, $\gamma = 1.0$, and strength $T\Delta\epsilon \sim 450$ K) and can be fitted with the same T_0 parameter as the corresponding α-process, which implies that both processes freeze at the same temperature. The VFT parameters for the α-process of all three samples are summarized in Table 2. A significant characteristic of the slower process is that its relaxation times scale with the α-process for $T \gg T_g$ being about 3 orders of magnitude slower ($\tau_{slow}/\tau_a \sim 10^3$) independent of the molecular weight. Clearly, the slower process does not relate to the flow of the system, but to an internal length scale. In a subsequent section we discuss the P dependence of this process. Recent NMR investigations on poly(*n*-alkyl methacrylates)[30] identified a new process between the usual segmental relaxation and the longest chain relaxation. This intermediate process reflects the randomization/isotropization of extended chain sequences and was typically 1−2 orders of magnitude slower than the segmental process at $T_g + 100$ K. However, by decreasing T, it merged with the faster α-process so that both froze at the same temperature (T_g), similarly with the slower process in P2VP.

To comment on the origin of the glass transition in P2VP, we employ pressure as an additional thermodynamic parameter. The P dependence of the relaxation times corresponding to the α- and slower processes in P2VP-B are shown in Figure 7. The two processes

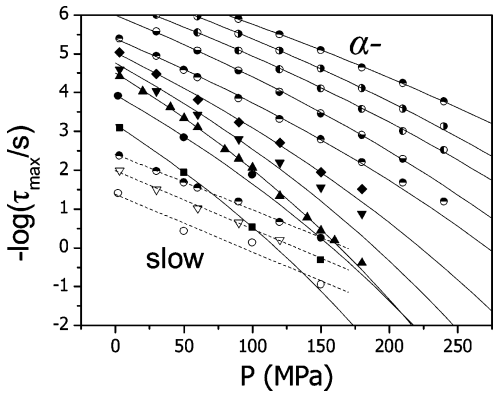

Figure 7. Relaxation times of the α- (filled and half-filled symbols) and the slower processes (open symbols) for the P2VP-B sample ($M_n = 9.0 \times 10^3$ g/mol), plotted against pressure for various "isotherms": (■) $T = 383.15$ K, (●, ○) $T = 393.15$ K, (▲) $T = 398.15$ K, (▼, ▽) $T = 403.15$ K, (◆) $T = 408.15$ K, (▲, △) $T = 413.15$ K, (▼) $T = 423.15$ K, (◧) $T = 433.15$ K, (◨) $T = 443.15$ K, (◓) $T = 453.15$ K. Solid lines are fits to eq 7, whereas dashed lines represent linear fits to the slower process $\tau(P)$ (see text).

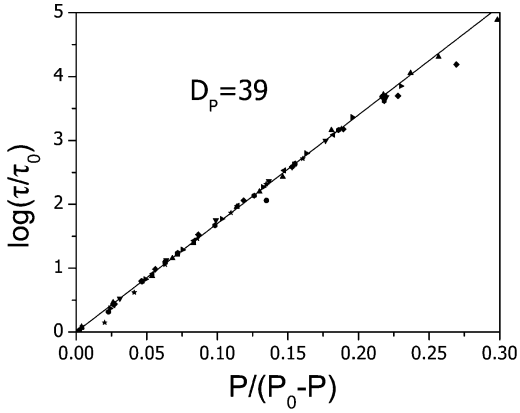

Figure 8. "Linearization"of the P-dependent VFT equation (eq 7). The τ_0 and P_0 parameters were obtained from the fit while keeping $D_P = 39$.

display a different P dependence and approach each other by increasing pressure, implying that they freeze at the same finite pressure; i.e., there exist both a common freezing temperature under "isobaric" conditions and a common freezing pressure under "isothermal" conditions. The "isothermal" relaxation times for the segmental relaxation have been fitted with the modified VFT equation for P dependence[31]

$$\tau_{\max} = \tau_0 \exp\left(\frac{D_P P}{P_0 - P}\right) \tag{7}$$

where D_P is a dimensionless parameter and P_0 the "ideal" glass pressure. Because of the limited curvature of $\tau(P)$, D_P was kept fixed to its value at 403.15 K ($D_P = 39$). To verify that this choice was correct, we "linearized" the VFT equation and plotted the data in Figure 8. All $\tau(T,P)$ points fall on a straight line with $D_P = 39$.

The data shown above allow us to divide the $T-P$ plane in three regimes; the "ideal" glass below T_0 (or equivalently below P_0), the normal glass between T_0 and T_g (or P_0 and P_g) and the melt. Figure 9 shows the $T-P$ points obtained from the fits above which correspond to the "normal" glass and the "ideal" glass transition. The glass transition temperatures obtained from PVT

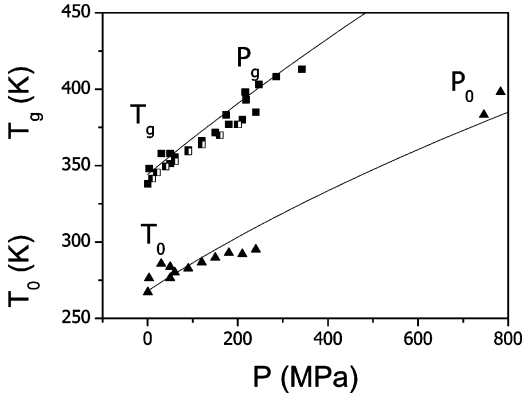

Figure 9. "Phase diagram" of the P2VP-B: (◧) T_g obtained from PVT (Figure 3); (■) T_g obtained from "isobaric" DS relaxation times and P_g values obtained by "isothermal" DS relaxation times; (▲) T_0 and P_0 values from the VFT fits corresponding to "isobaric" and "isothermal" conditions, respectively. The lines are fits according to eq 8.

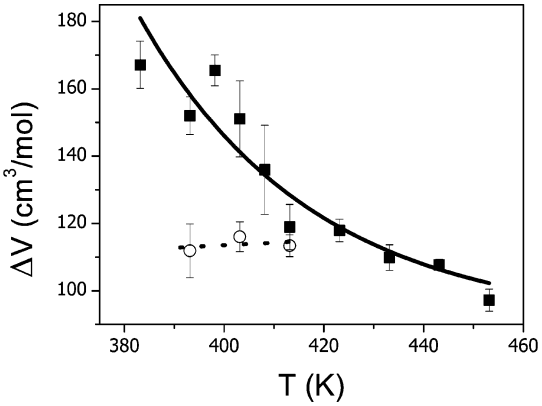

Figure 10. Apparent activation volume as a function of temperature for the α- (■) and the slower (○) processes of P2VP-B ($M_n = 9.0 \times 10^3$ g/mol). Note that the apparent activation volume corresponding to the α-process approaches the monomer volume (109 cm^3/g) at high temperatures but increases rapidly by decreasing T toward T_g. Note the insensitivity of $\Delta V(T)$ for the slower process.

have also been included and are in excellent agreement with the results from the dynamic study. The points at the borders of the phases have been fitted using the empirical equation[6]

$$T = a\left(1 + \frac{b}{c}P\right)^{(1/b)} \tag{8}$$

where $a = T(0)$ and b, c are constants. These parameters assume the following values for P2VP-B: $a = 337$ K (268 K), $b = 8.8$ (2.36), and $c = 9.8 \times 10^2$ MPa (1.40×10^3) for $T_g(P)$ ($T_0(P)$). The initial slope (at 0.1 MPa) of the curve corresponding to the glass transition is $(dT_g/dP)_{P\to 0} = 0.34$ K/MPa. Notice that the pressure coefficient in P2VP is similar to that of polystyrene, with a similar structure (same backbone and side group composed of an aromatic ring), as $(dT_g/dP)_{P\to 0} = 0.36$ K/MPa in PS.[32]

The apparent activation volume of the α-relaxation process is defined as[9]

$$\Delta V = RT\left(\frac{\partial \ln \tau_{max}}{\partial P}\right)_T \tag{9}$$

and in a broader sense it could be considered as a measure of the volume associated with the relaxation. Figure 10 shows the activation volume for the α- and the slower process of P2VP-B. At temperatures slightly above T_g, the activation volume for the α-process is very high but falls rapidly by increasing temperature and approaches the monomer volume (109 cm^3/g) at $T \sim T_g + 70$ K. On the other hand, the activation volume corresponding to the slower process is nearly constant and equal to the monomer volume.

The PVT data allow the construction of a "density representation" where the dielectric relaxation times can be plotted as a function of density (Figure 11). The dashed and solid lines are fits of the "isothermal" and "isobaric" data sets, respectively, with the modified VFT equation for the density representation[5]

$$\tau_{max} = \tau_0 \exp\left(\frac{D_\rho \rho}{\rho_0 - \rho}\right) \tag{10}$$

where D_ρ is a dimensionless parameter and ρ_0 is the density at the "ideal" glass. The density representation is very useful in testing the validity of the free volume

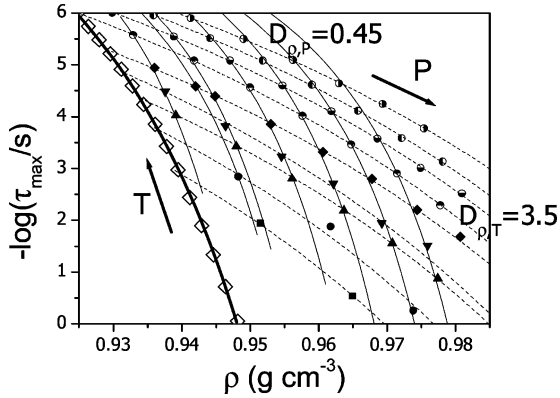

Figure 11. Relaxation times plotted against density using the Tait equation (eq 1). The dashed and the solid lines are fits to the "isothermal" and "isobaric" data, respectively, using eq 9 ($D_{\rho P} = 0.45$, $D_{\rho T} = 3.5$ are the values of the respective parameters). The "isotherms" are at (■) $T = 383.15$ K, (●) $T = 393.15$ K, (▲) $T = 403.15$ K, (▼) $T = 408.15$ K, (♦) $T = 413.15$ K, (▲) $T = 423.15$ K, (▼) $T = 433.15$ K, (▽) $T = 443.15$ K, (◊) $T = 453.15$ K. The relaxation times at $P = 0.1$ MPa are also shown ((◒) $P = 0.1$ MPa).

theories, which predict that volume is the main thermodynamic parameter controlling the dynamics. Assuming that the fraction of free volume and the specific volume have a one-to-one correspondence, then the simplest free volume theory would predict no change of the segmental relaxation times under isochoric conditions. The relative contribution of volume and thermal effects to the dynamic response can be obtained by calculating the ratio of the activation energies under constant density or volume $Q_V = -RT^2(\partial \ln \tau_{max}/\partial T)_V$ and constant pressure $Q_P = -RT^2(\partial \ln \tau_{max}/\partial T)_P$. This ratio lies in the range 0−1. A value of zero indicates that volume is the main controlling parameter of the dynamics, whereas a value near one suggests thermal energy as the controlling parameter, instead.

It can be shown that the ratio Q_V/Q_P can be obtained directly from Figure 11 as

$$\frac{Q_V}{Q_P} = 1 - \frac{\left(\frac{\partial \ln \tau_{max}}{\partial \rho}\right)_T}{\left(\frac{\partial \ln \tau_{max}}{\partial \rho}\right)_P} \tag{11}$$

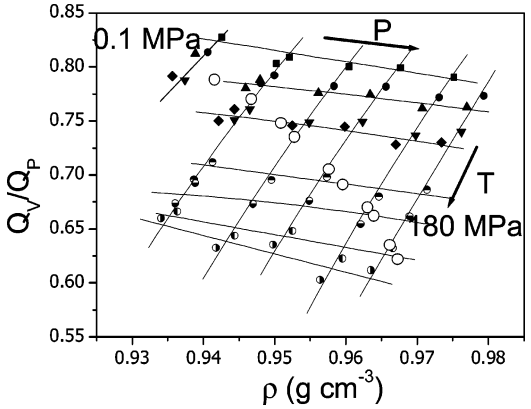

Figure 12. Ratio of the activation energies under constant volume and under constant pressure plotted against density. The arrows show the direction of increasing temperature and pressure for the "isobaric" and "isothermal" sets, respectively. The "isothermal" data are at (■) $T = 383.15$ K, (●) $T = 393.15$ K, (▲) $T = 403.15$ K, (▼) $T = 408.15$ K, (♦) $T = 413.15$ K, (▲) $T = 423.15$ K, (▼) $T = 433.15$ K, (▽) $T = 443.15$ K, (◊) $T = 453.15$ K.

without any extrapolations. The thus-obtained values of the ratio Q_V/Q_P for the different (P, T) conditions are plotted in Figure 12 as a function of density. As seen in that figure, the ratio assumes values in the range 0.6−0.85 under the different (T, P) conditions investigated, i.e., within the T range $T_g + 43$ K to $T_g + 113$ K and within the P range 0.1−270 MPa. Increasing pressure up to 270 MPa under "isothermal" conditions has a negligible effect on the ratio, but decreasing temperature under "isobaric" conditions causes the ratio to rise rapidly, meaning that thermal effects control the dynamics at temperatures close to T_g. We mention here that for poly(propylene oxide)[33] Q_V/Q_P was increasing upon isothermal densification while it was decreasing by isobaric densification. For P2VP, at $T = T_g + 30$ K (i.e., $\tau_{max} \sim 10^{-2}$ s) and $P = 0.1$ MPa, the ratio assumes values in the vicinity of 0.78. The same ratio can be calculated independently from[34]

$$\frac{Q_V}{Q_P} = 1 - \left(\frac{\partial P}{\partial T}\right)_V \left(\frac{\partial T}{\partial P}\right)_\tau \qquad (12)$$

where $(\partial P/\partial T)_V$ is obtained from PVT and $(\partial T/\partial P)_\tau$ is the pressure coefficient of T_g. Using $(\partial P/\partial T)_V|_{\tau=1s} = 0.89$ MPa/K, $(\partial P/\partial T)_V|_{\tau=100s} = 0.74$ MPa/K, and $(\partial T/\partial P)_{\tau\sim1s} = (\partial T/\partial P)_{\tau\sim100s} = (\partial T_g/\partial P)_{P\to0} = 0.34$ K/MPa, we obtain 0.70 and 0.75 for the ratio from eq 12, for $P = 0.1$ MPa and $\tau = 1$ and 100 s, respectively. This value is higher than for the structurally similar PS ($Q_V/Q_P \sim 0.64$)[32] with a LVDW peak at $q^* \sim 8$ nm^{-1} (suggesting similar packing conditions). The increased contribution of temperature relative to volume in P2VP, as compared to PS, could reflect the influence of hydrogen bonding (C−H···N) with a strength of 12−20 kJ/mol, which is absent in PS.

The existence of the $\tau(P)$ relaxation times for the slower process allow an estimation of the ratio Q_V/Q_P using the formalism described above with respect to eq 11. Although the data are less accurate in this case, they still allow for an estimation of its value. At $T_g + 30$ K and $P = 0.1$ MPa, we obtain a value of 0.77 ± 0.1, which is similar to the one for the segmental process. Therefore, the dynamics of the slower process are also governed by thermal energy mainly as opposed to the available volume.

IV. Conclusions

The investigation of the dynamics in three P2VP samples with different molecular weights revealed three dielectrically active processes: (i) a weak process well below T_g, reflecting the localized motion of the pyridine group and/or a reduced number of relaxing units with an activation energy of 53 kJ/mol (independent of chain length), (ii) the usual segmental process freezing at T_g, and (iii) a slower process (typically $\tau_s/\tau_a \sim 10^3$ at $T \gg T_g$) that follows a VFT T dependence and freezes, respectively, at the same temperature and pressure under "isobaric" and "isothermal" conditions as the segmental process. The latter process was found to have a temperature-independent apparent activation volume that is comparable to the monomer volume, whereas the apparent activation volume associated with the α-process displays a strong T dependence.

With respect to the origin of the glass transition, the main results are summarized below:

(i) The principle of time−temperature−pressure superposition works reasonably well only around the α-process maximum.

(ii) The dynamic arrest at T_g is caused both by the reduction in thermal energy and by the unavailable free volume. A quantitative comparison of the activation energies under constant volume and under constant pressure revealed that their Q_V/Q_P ratio is 0.78 at $T_g + 30$ K and varies between 0.6 and 0.85 for the different T, P conditions investigated. This result clearly shows that temperature has a stronger influence than volume in determining the segmental relaxation times especially as temperature is lowered toward T_g. A similar value (0.77) was estimated for the slower process at the same conditions, implying that the dynamics of the slower process are also controlled primarily by thermal energy.

(iii) The $T-P$ plane can be separated in three regimes according to the segmental process relaxation times: the "ideal" glass state in which the segmental process freezes, the "normal glass" where the segmental relaxation time is greater than 100 s, and the melt.

Acknowledgment. P.P. and G.F. thank the GSRT for a grant (PENED2001). We are indebted to A. Best at the Max-Planck Institute for Polymer Research for the PVT measurements and G. Tsoumanis (UoI) for technical support.

References and Notes

(1) Ngai, K. L., Floudas, G., Rizos, A. K., Riande, E., Eds. Proceedings of the Fourth International Discussion Meeting on Relaxations in Complex Systems; *J. Non-Cryst. Solids* **2002**, *307−310*. Ngai, K. L., Riande, E., Eds. Proceedings of the Third International Discussion Meeting on Relaxations in Complex Systems; *J. Non-Cryst. Solids* **1998**, *235−237*. Ngai, K. L., Riande, E., Wright, G. B., Eds. Proceedings of the Second International Discussion Meeting on Relaxations in Complex Systems; *J. Non-Cryst. Solids* **1994**, *172−174*. Ngai, K. L., Wright, G. B., Eds. Proceedings of the First International Discussion Meeting on Relaxations in Complex Systems; *J. Non-Cryst. Solids* **1991**, *131−133*.
(2) Williams, G. *Trans. Faraday Soc.* **1966**, *62*, 2091.
(3) Sasabe, H.; Saito, S. *J. Polym. Sci., Part A-2* **1968**, *6*, 1401.
(4) Floudas, G.; Reisinger, T. *J. Chem. Phys.* **1999**, *111*, 5201.
(5) Floudas, G.; Gravalides, C.; Reisinger, T.; Wegner, G. *J. Chem. Phys.* **1999**, *111*, 9847.
(6) Andersson, S. P.; Andersson, O. *Macromolecules* **1998**, *31*, 2999.
(7) Kirpatch, A.; Adolf, D. B. *Macromolecules* **2004**, *37*, 1576.
(8) Floudas, G.; Fytas, G.; Reisinger, T.; Wegner, G. *J. Chem. Phys.* **1999**, *111*, 9129.

(9) Floudas, G. In *Broadband Dielectric Spectroscopy*; Kremer, F., Schönhals, A., Eds.; Springer: Berlin, 2002; Chapter 9.
(10) Alegria, A.; Gomez, D.; Colmenero, J. *Macromolecules* **2002**, *35*, 2030.
(11) Zhang, S. H.; Casalini, R.; Runt, J.; Roland, C. M. *Macromolecules* **2003**, *36*, 9917.
(12) Mierzwa, M.; Floudas, G.; Stepanek, P.; Wegner, G. *Phys. Rev. B* **2000**, *62*, 14012.
(13) Mierzwa, M.; Floudas, G. *IEEE Trans. Dielectr. Insul.* **2001**, *8*, 359.
(14) Mierzwa, M.; Floudas, G.; Neidhoefer, M.; Graf, R.; Spiess, H. W. Meyer, W. H.; Wegner, G. *J. Chem. Phys.* **2002**, *117*, 6289.
(15) Gitsas, A.; Floudas, G.; Wegner, G. *Phys. Rev. E* **2004**, *69*, 041802.
(16) Floudas, G.; Mierwza, M.; Schönhals, A. *Phys. Rev. E* **2003**, *67*, 031705.
(17) Floudas, G.; Papadopoulos, P.; Klok, H.-A.; Vandermeulen, G. W. M.; Rodriguez-Hernandez, J. *Macromolecules* **2003**, *36*, 3673.
(18) Williams, G. *Trans. Faraday Soc.* **1964**, *60*, 1556.
(19) Ferrer, M. L.; Lawrence, C.; Demirjian, B. G.; Kivelson, D.; Alba-Simionesco, C.; Tarjus, G. *J. Chem. Phys.* **1998**, *109*, 8010.
(20) Casalini, R.; Roland, C. M. *J. Chem. Phys.* **2003**, *119*, 4052.
(21) Roland, C. M.; Paluch, M.; Pakula, T.; Casalini, R. *Philos. Mag.* **2004**, *84*, 1573.
(22) Mpoukouvalas, K.; Floudas, G. *Phys. Rev. E* **2003**, *68*, 031801.
(23) Paluch, M.; Casalini, R.; Patkowski, A.; Pakula, T.; Roland, C. M. *Phys. Rev. E* **2003**, *68*, 031802.
(24) Floudas, G.; Stepanek, P. *Macromolecules* **1998**, *31*, 6951.
(25) Floudas, G.; Pakula, T.; Stamm, M.; Fischer, E. W. *Macromolecules* **1993**, *26*, 1671.
(26) Mierzwa, M.; Floudas, G.; Wegner, G. *Diel. Newsletter* **2000** (June).
(27) Havriliak, S.; Negami, S. *Polymer* **1967**, *8*, 161.
(28) Wübbenhorst, M.; van Koten, E.; Jansen, J.; Mijw, M.; van Turnhout, J. *Macromol. Rapid Commun.* **1997**, *18*, 139.
(29) Richert, R.; Wagner, H. *Solid State Ionics* **1998**, *105*, 167.
(30) Wind, M.; Graf, R.; Heuer, A.; Spiess, H. W. *Phys. Rev. Lett.* **2003**, *91*, 155702.
(31) Paluch, M.; Patkowski, A.; Fischer, E. W. *Phys. Rev. Lett.* **2000**, *85*, 2140.
(32) Roland, C. M.; Casalini, R. *J. Chem. Phys.* **2003**, *119*, 1838.
(33) Williams, G. *Trans. Faraday Soc.* **1965**, *61*, 1564.
(34) Naoki, M.; Endou, H.; Matsumoto, K. *J. Phys. Chem.* **1987**, *91*, 4169.

MA048555S